Increased atrial effectiveness of flecainide conferred by altered biophysical properties of sodium channels

O'Brien, Sian-Marie; Holmes, Andy; Johnson, Daniel; Kabir, Syeeda Nashitha; O'Shea, Christopher; O'Reilly, Molly; Avezzu, Adelisa; Reyat, Jasmeet; Hall, Amelia W.; Apicella, Clara; Ellinor, Patrick T. ; Niederer, Steven; Tucker, Nathan R. ; Fabritz, Larissa; Kirchhof, Paulus; Pavlovic, Davor

DOI:
10.1016/j.yjmcc.2022.01.009

Document Version
Publisher's PDF, also known as Version of record

Citation for published version (Harvard):
O'Brien, S-M, Holmes, A, Johnson, D, Kabir, SN, O'Shea, C, O'Reilly, M, Avezzu, A, Reyat, J, Hall, AW, Apicella, C, Ellinor, PT, Niederer, S, Tucker, NR, Fabritz, L, Kirchhof, P & Pavlovic, D 2022, 'Increased atrial effectiveness of flecainide conferred by altered biophysical properties of sodium channels', *Journal of Molecular and Cellular Cardiology*, vol. 166, pp. 23-35. https://doi.org/10.1016/j.yjmcc.2022.01.009

Journal of Molecular and Cellular Cardiology 166 (2022) 23–35

Contents lists available at ScienceDirect

Journal of Molecular and Cellular Cardiology

journal homepage: www.elsevier.com/locate/yjmcc

Increased atrial effectiveness of flecainide conferred by altered biophysical properties of sodium channels

Sian O' Brien [a,1], Andrew P. Holmes [a,b,1], Daniel M. Johnson [a,c], S. Nashitha Kabir [a], Christopher O' Shea [a], Molly O' Reilly [a], Adelisa Avezzu [d], Jasmeet S. Reyat [a], Amelia W. Hall [e,f], Clara Apicella [a], Patrick T. Ellinor [e,f], Steven Niederer [d], Nathan R. Tucker [e,f,g], Larissa Fabritz [a,h,i,j], Paulus Kirchhof [a,i,j], Davor Pavlovic [a,*]

[a] Institute of Cardiovascular Science, University of Birmingham, Birmingham, UK
[b] School of Biomedical Sciences, Institute of Clinical Sciences, University of Birmingham, Birmingham, UK
[c] School of Life, Health and Chemical Sciences, The Open University, Walton Hall, Milton Keynes, UK
[d] School of Biomedical Engineering & Imaging Sciences, Kings' College London, London, UK
[e] Cardiovascular Research Center, Massachusetts General Hospital, Boston, MA 02129, USA
[f] Cardiovascular Disease Initiative, The Broad Institute of MIT and Harvard, Cambridge, MA 02142, USA
[g] Masonic Medical Research Institute, Utica, NY, 13501, USA
[h] University Center of Cardiovascular Science, University Heart and Vascular Center UKE, Hamburg, Germany
[i] Department of Cardiology, University Heart and Vascular Center UKE, Hamburg, Germany
[j] German Center for Cardiovascular Research (DZHK), Partner Site Hamburg/Kiel/Lübeck, Germany

ARTICLE INFO

Keywords:
Atria
Ventricles
Sodium channels
Flecainide
Conduction

ABSTRACT

Atrial fibrillation (AF) affects over 1% of the population and is a leading cause of stroke and heart failure in the elderly. A feared side effect of sodium channel blocker therapy, ventricular pro-arrhythmia, appears to be relatively rare in patients with AF. The biophysical reasons for this relative safety of sodium blockers are not known.

Our data demonstrates intrinsic differences between atrial and ventricular cardiac voltage-gated sodium currents (I_{Na}), leading to reduced maximum upstroke velocity of action potential and slower conduction, in left atria compared to ventricle. Reduced atrial I_{Na} is only detected at physiological membrane potentials and is driven by alterations in sodium channel biophysical properties and not by $Na_V1.5$ protein expression. Flecainide displayed greater inhibition of atrial I_{Na}, greater reduction of maximum upstroke velocity of action potential, and slowed conduction in atrial cells and tissue.

Our work highlights differences in biophysical properties of sodium channels in left atria and ventricles and their response to flecainide. These differences can explain the relative safety of sodium channel blocker therapy in patients with atrial fibrillation.

1. Introduction

Atrial fibrillation (AF) is a common cardiac arrhythmia and a major driver of stroke, heart failure, and cardiovascular death. Incidence and prevalence of AF is expected to increase further, with projected estimates of 6 million AF patients in US and 17.9 million in Europe, over the next 30–40 years [1,2].

Sodium channel blockers such as flecainide are commonly used to restore rhythm in patients with AF. These were initially developed to suppress ventricular arrhythmias. Following the increased mortality found in the CAST trial comparing flecainide and encainide to placebo [3], flecainide and similar agents are now primarily used for rhythm control therapy of patients with atrial fibrillation (AF) with normal ventricular function and without ischemic heart disease [4–8]. Recent

Abbreviations: RMP, resting membrane potential; AF, Atrial Fibrillation; LA, Left atrium; LV, Left ventricle; CV, Conduction velocity.

* Corresponding author at: Institute of Cardiovascular Science, University of Birmingham, Birmingham B15 2TT, UK.
E-mail address: d.pavlovic@bham.ac.uk (D. Pavlovic).

[1] These authors share first authorship.

https://doi.org/10.1016/j.yjmcc.2022.01.009
Received 19 November 2021; Received in revised form 13 January 2022; Accepted 26 January 2022
Available online 1 February 2022

controlled trials (Flec-SL and EAST-AFNET 4) demonstrate a low rate of ventricular pro-arrhythmia when flecainide is used after cardioversion and during long-term rhythm control therapy as part of an early rhythm control strategy, including in patients with heart failure with preserved ejection fraction [4,9,10]. This contrasts with the ventricular pro-arrhythmia observed when flecainide was used to suppress ventricular arrhythmias in patients with myocardial ischemia [3]. The reasons for this discrepancy are unclear and with the predicted increase in use of early rhythm therapy, as a consequence of the EAST-AFNET 4 trial, better understanding of the effects of flecainide on atrial and ventricular electrical function is waranted.

Although flecainide has been shown to inhibit the rapid delayed rectifier current at clinically relevant doses, which may account for some proarrhythmic outcomes, flecainide primarily inhibits myocardial Na^+ channels, of which $Na_V1.5$ is the primary pore-forming alpha subunit found in mammalian heart [11–15]. $Na_V1.5$ is a large transmembrane protein primarily mediating the cardiac Na^+ current (I_{Na}) in cardiac cells. Localization and plasma membrane expression of the $Na_V1.5$ is reliant on specific beta subunits [16] and $Na_V\beta2$ and $Na_V\beta4$ subunits can modulate the kinetic and voltage dependence properties of the I_{Na} [17]. Flecainide is known to block $Na_V1.5$ in its open, activated state, where it can bind to the pore and prevent Na^+ from traversing the membrane [18,19]. This leads to enhanced refractoriness especially at rapid atrial rates, as seen in AF [20]. However, inhibition of Na^+ channels also slows conduction velocity, which can both terminate multiple reentry and increase the predisposition to functional conduction block and macro-reentrant arrhythmias [21,22]. Functional conduction block and macro-reentry are believed to contribute to the ventricular pro-arrhythmia found in the CAST trial studying flecainide, encanide, and moricizine in survivors of a myocardial infarction with reduced left ventricular function.

Several crucial questions remain unanswered, regarding flecainide and atrial and ventricular electrical function. It is not known whether flecainide exhibits differential sodium channel-blocking effects in atria and ventricles. Characterization of the atrial and ventricular conduction differences are yet to be studied in the same hearts, or indeed the extent of conduction slowing caused by flecainide. Chamber differences in peak I_{Na} when measured over a range of different holding potentials remains to be determined, as well as the sensitivity to flecainide. Whilst increased peak I_{Na} is reported in cells isolated from left atrium (LA) compared to those isolated from left ventricle (LV) [23–27], it is not clear if this is conserved at more physiological resting membrane potentials (RMPs), which are likely to differentially impact on sodium channel availability, gating and flecainide efficacy. Furthermore, it is not known if chamber differences in expression of *SCN5a*/Nav1.5, *SCN2B*/$Na_V\beta2$ and *SCN4B*/$Na_V\beta4$ exist and if they are consistent in healthy murine and human heart tissue.

The aims of the present study were to robustly interrogate differences in biophysical properties of ventricular and atrial I_{Na} (inclusive of measurements at physiological membrane potentials), their effects on conduction, and examine chamber specific responses to flecainide. Furthermore, we investigated expression profiles of sodium channel subunits in atrial and ventricular chambers in non-failing murine and human tissue.

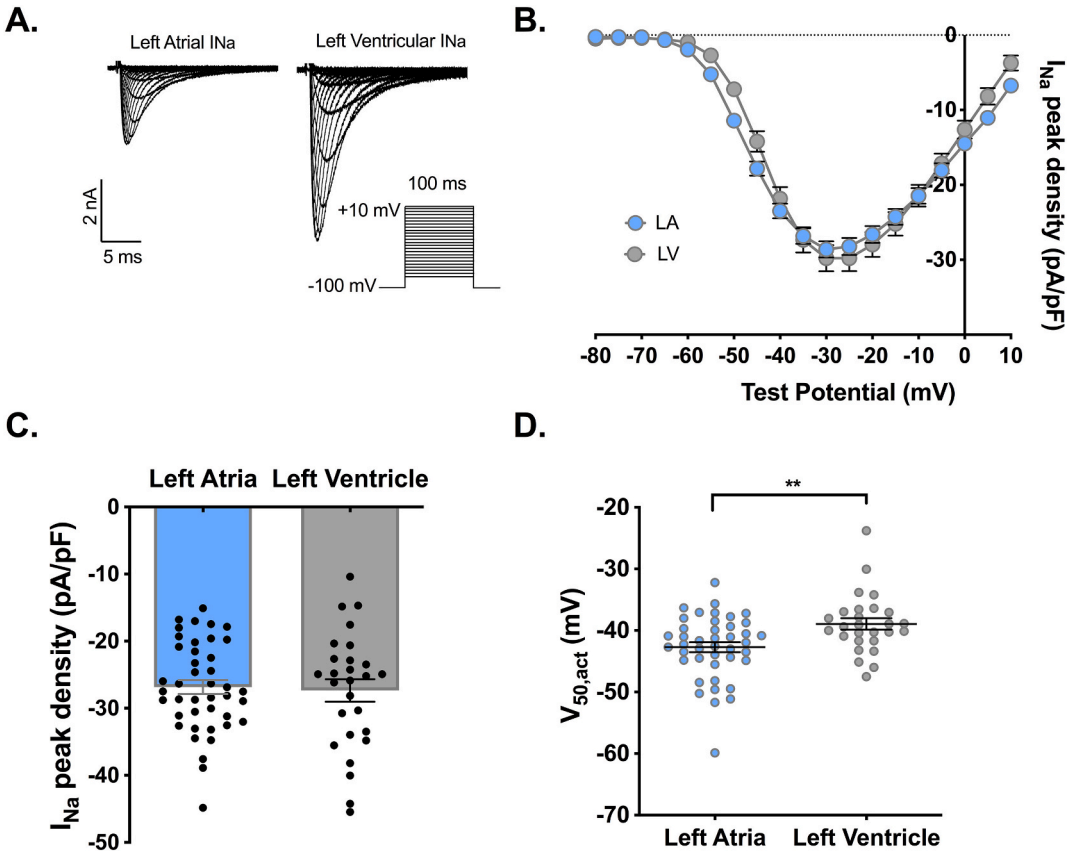

Fig. 1. Left atrial (LA) and left ventricular (LV) I_{Na} current/voltage relationship and sodium channel activation. A) Representative raw I_{Na} traces from LA and LV cardiomyocytes, inset indicates voltage protocol. B) Current voltage relationship of INa peak density in LA and LV. C) I_{Na} peak density at a step from -100 mV to -30 mV in LA (−27.4 ± 1.7 pA/pF) and LV (−26.8 ± 1.0 pA/pF); $p = 0.785$. D) $V_{50,act}$ fitted to the Boltzmann distribution in LA (−42.7 ± 0.8 mV;) and LV (−38.6 ± 0.9 mV). Each dot represents an individual cell, $^{**}p < 0.01$, (Two-way nested ANOVA). $^{**}P < 0.01$, $n = 42/13$ cells/mice for LA and $n = 28/13$ cells/mice for LV.

2. Results

2.1. Biophysical properties of I_{Na} differ between the left ventricle and left atrium

We first set out to quantitatively compare I_{Na} in adult murine cardiomyocytes isolated from left atria and left ventricles. To measure peak I_{Na}, we initially employed a standard protocol, where I_{Na} was elicited from a holding potential of -100 mV. Example raw I_{Na} traces are demonstrated in Fig. 1A. When normalized to capacitance (**Supplemental Fig. 1**) and measured from a holding potential of -100 mV no differences in I_{Na} density were seen between the left atria and left ventricles at any test potential (Fig. 1B,C). However, atrial cardiomyocytes exhibited an approximately 4 mV more negative $V_{50,act}$, compared to ventricular cardiomyocytes (Fig. 1D). We also examined whether differences in the I_{Na} inactivation kinetics exist in datasets in Fig. 1. Time to peak and time to 95% decay were increased in left ventricular cardiomyocytes compared to atrial (time to peak - LA 0.86 ± 0.03 ms, LV 1.16 ± 0.06 ms; ****$p \leq 0.0001$ unpaired *t*-test, $n = 30$ cells for LA and $n = 29$ cells for LV), (time to 95% decay - LA 4.25 ± 0.23 ms, LV 6.47 ± 0.24 ms; ****p ≤ 0.0001 unpaired t-test, n = 30 cells for LA and n = 29 cells for LV). These differences however are likely driven by larger ventricular currents.

Under normal physiological conditions, cardiomyocytes are not at a resting membrane voltage of -100 mV or -120 mV (conditions at which I_{Na} is usually measured), however the resting membrane potential lies in the range of −90 to -65 mV [28,29]. Thus, the magnitude of I_{Na} over this physiological range will depend not only on the population size of functional $Na_V1.5$ channels but also on the number of channels that are available to conduct ions at a given resting membrane voltage. Therefore, we went on to determine how resting membrane potential could alter the peak I_{Na} current (Fig. 2A**)**. The holding potential had a marked and differential effect on the left atrial and left ventricular I_{Na}. At a holding potential of -120 mV, atrial peak I_{Na} was larger (−35.7 ± 1.3 pA/pF, n = 40/13 cells/mice) when compared to ventricular cardiomyocytes (−30.9 ± 1.7, p = 0.027, Fig. 2B). However, this was reversed when sodium channels were activated from a more physiologically relevant holding potential of -75 mV; peak current density was lower in left atrial cardiomyocytes (6.7 ± 0.8 pA/pF, n = 40/13 cells/mice) when compared to the ventricular cardiomyocytes (9.7 ± 1.1pA/pF, n = 28/13 cells/mice, p = 0.026), Fig. 2C. Thus, although atrial cardiomyocytes have a greater maximal I_{Na} density when activated from −120 mV, the physiologically relevant I_{Na} size is actually significantly lower in atrial than ventricular cardiomyocytes.

Voltage dependent steady state inactivation of I_{Na} is critical to the function of the cardiomyocyte as it determines the number of available $Na_V1.5$ channels, and thus can have major effects on peak depolarizing current, conduction and interactions with pharmacological agents. Left atrial I_{Na} inactivated at significantly more negative voltages than in left ventricular cardiomyocytes, with significant differences observed over a wide range of voltages (**Supplemental Fig. 2A**). The mean voltage of half-maximal steady-state inactivation ($V_{50,\ inact}$) of the atrial cardiomyocytes was 6.5 ± 1.5 mV more negative than that of ventricular cardiomyocytes (**Supplemental Fig. 2B**). This has important physiological consequences; at −120 mV there was no difference in steady-state inactivation %, as nearly all channels are available. However, at

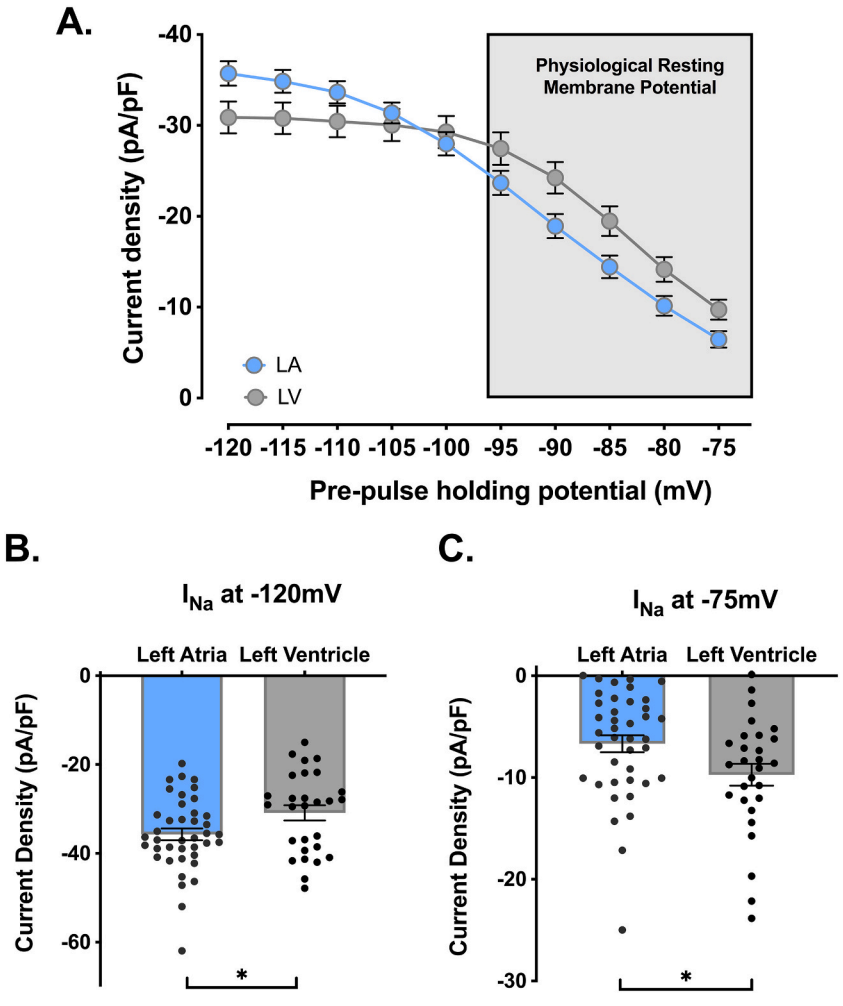

Fig. 2. INa density at varying holding potentials from left atrial (LA) and left ventricular (LV) cardiomyocytes. A) INa mean density/holding potential relationship, LA (n = 40/13 cells/mice) and LV (n = 28/13 cells/mice). The range of the physiological resting membrane potential is highlighted in grey. Voltage protocol shown in inset. B) INa density at -120 mV holding potential in LA (−35.7 ± 1.3 pA/pF; n = 40/13 cells/mice) and in LV (−30.9 ± 1.7 pA/pF; n = 28/13 cells/mice, *$p < 0.05$). Each dot represents an individual cell, **p < 0.01, (Two-way nested ANOVA). C) I_{Na} density at -75 mV holding potential in LA (−6.7 ± 0.8 pA/pF; n = 40/13 cells/mice) and LV (−9.7 ± 1.1 pA/pF; n = 28/13 cells/mice, *p < 0.05) Each dot represents an individual cell, **$p < 0.01$, (Two-way nested ANOVA).

less negative voltages, inactivation % is greater in the LA when compared to the LV. For example, at −90 mV, 47.7 ± 3.3% of channels were no longer available for activation in the LA, compared to only 24.8 ± 2.6% in the LV ($p < 0.0001$). At a more physiological potential of −75 mV, the difference in inactivated channels between the left atria (82 ± 2.2%) and left ventricles (71.8 ± 2.8%, $P < 0.0049$, **Supplemental Fig. 2C**) is significant. Voltage inactivation slope constants (k) were consistent between LA (7 ± 0.3, $N = 12$) and LV (6.9 ± 0.1, $N = 19$, $P \geq 0.05$).

Recovery from inactivation was examined using a double pulse, P1 and P2 protocol that delivered two identical depolarizing pulses to −30 mV of 25 ms duration. Atrial I_{Na} was slower to recover from inactivation when comparing the P50 (time when half of the channels were recovered) of recovery in LA (22.6 ± 1.7 ms) and LV (15.5 ± 1.5 ms) (**Supplemental Fig. 3**). Recovery differences shown here are therefore likely to contribute to the reduced I_{Na} at physiological holding potentials, action potential upstroke and conduction in the atria, observed in this study.

In order to examine whether these differing I_{Na} characteristics can lead to alterations in action potential morphology, specifically action potential (AP) upstroke, we went on to include these biophysical data in a mathematical model of the ventricular cardiomyocyte [30]. As shown in Fig. 3, the modelling data fitted the experimental data well in terms of current activation and inactivation (Fig. 3A and B).

Incorporating the kinetics of the sodium channel from the left atrial and left ventricular cardiomyocytes resulted in a reduced current density in the 'atrial' cell as well as slower current decay during an AP when compared to the ventricular cell (Fig. 3C). There was also a slower peak maximum upstroke velocity (dV/dt) of the modelled 'atrial' cell compared to the ventricular cell (121.59 mV/ms for the LA when compared to 130.32 mV/ms for LV) and a smaller AP amplitude, when measured at 1 Hz pacing cycle length and an RMP of -80 mV, Fig. 3D. We followed these modelling experiments with current-clamp experiments on single isolated cardiac myocytes (Fig. 4) to determine the applicability of the modelling data. As shown in Fig. 4B, when paced at 1 Hz, left atrial myocytes had an RMP of 70.8 ± 1.4 mV, whereas left ventricular myocytes were generally less depolarized with an RMP of −74.4 ± 1.0 mV ($p = 0.0002$, $n = 23$–40/5 cells/mice). Furthermore, maximal upstroke velocity of the AP was significantly higher in single ventricular cells when compared to atrial cells (at 1 Hz, LA 238.6 ± 27.7 mV/ms; LV 304.2 ± 27.9 mV/ms *$p = 0.0018$, n = 23–40/5 cells/mice) (Fig. 4C).

2.2. Flecainide has a greater inhibitory effect in the left atrial cardiomyocytes

We investigated the effect of clinically relevant flecainide concentration (1 μM) on I_{Na} and action potential properties in atrial and ventricular cardiomyocytes. When activating I_{Na} from a fixed holding potential of −100 mV, flecainide inhibited I_{Na} to a larger extent in the atrial when compared to the ventricular cells (Fig. 5). For example, at a test potential of −35 mV, I_{Na} was inhibited by approximately 48% in the atria, Fig. 5B ((27.3 ± 3.1 pA/pf (control) to 14.1 ± 2.0 pA/pF (flecainide), $p < 0.0001$ $n = 11/6$ cells/mice)), whilst flecainide inhibited ventricular I_{Na} by approximately 38%, Fig. 5C ((27.0 ± 1.6 pA/pf

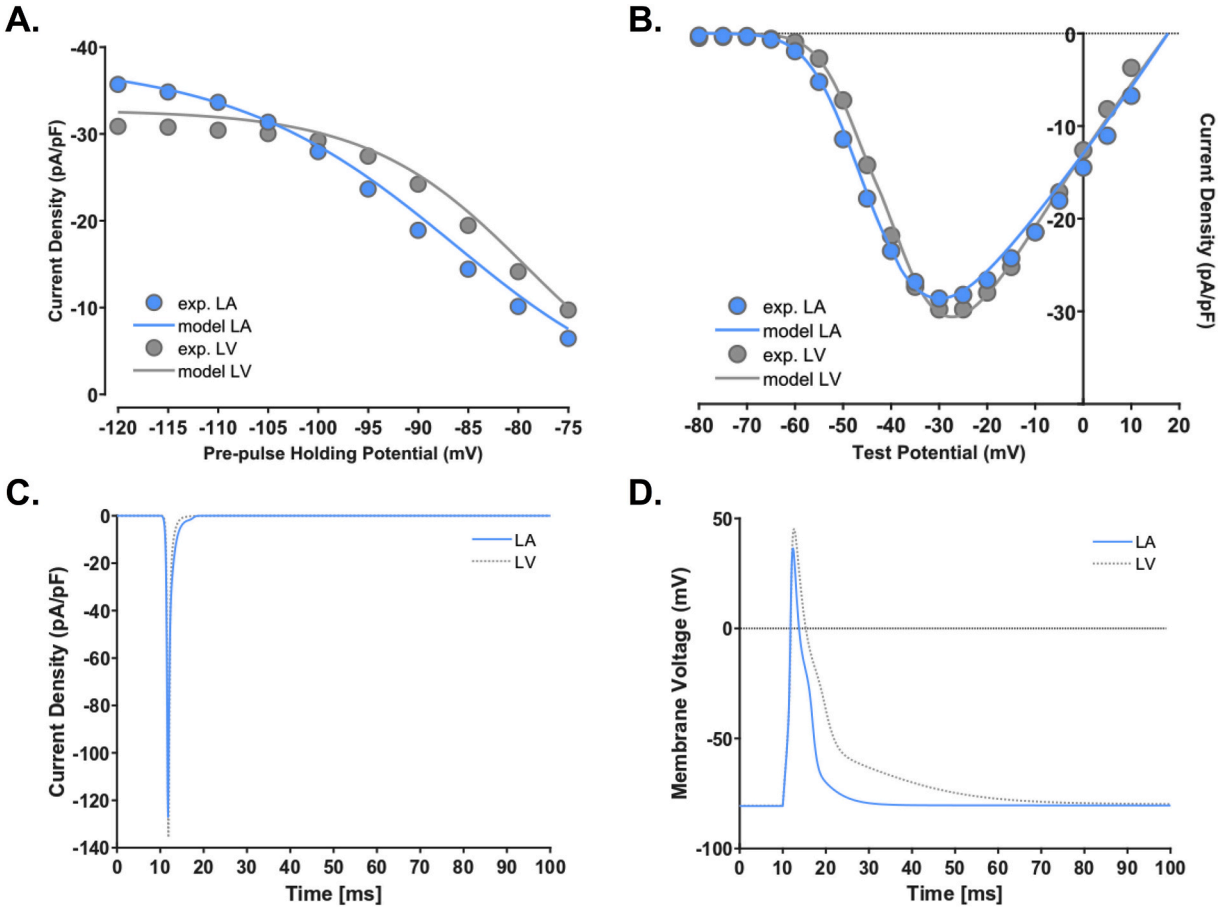

Fig. 3. Modelling data illustrates a larger ventricular I_{Na} current leading to larger action potential amplitude in ventricles during a modelled cardiac action potential. A) I_{Na} density at varying holding potentials from left atrial (LA) and left ventricular (LV) cardiomyocytes from the model and experimental data. B) LA and LV I_{Na} current/voltage relationship and sodium channel activation in both experimental and modelling data. C) I_{Na} generated during a modelled AP. D) Examples of modelled APs utilizing the LA and LV I_{Na} data.

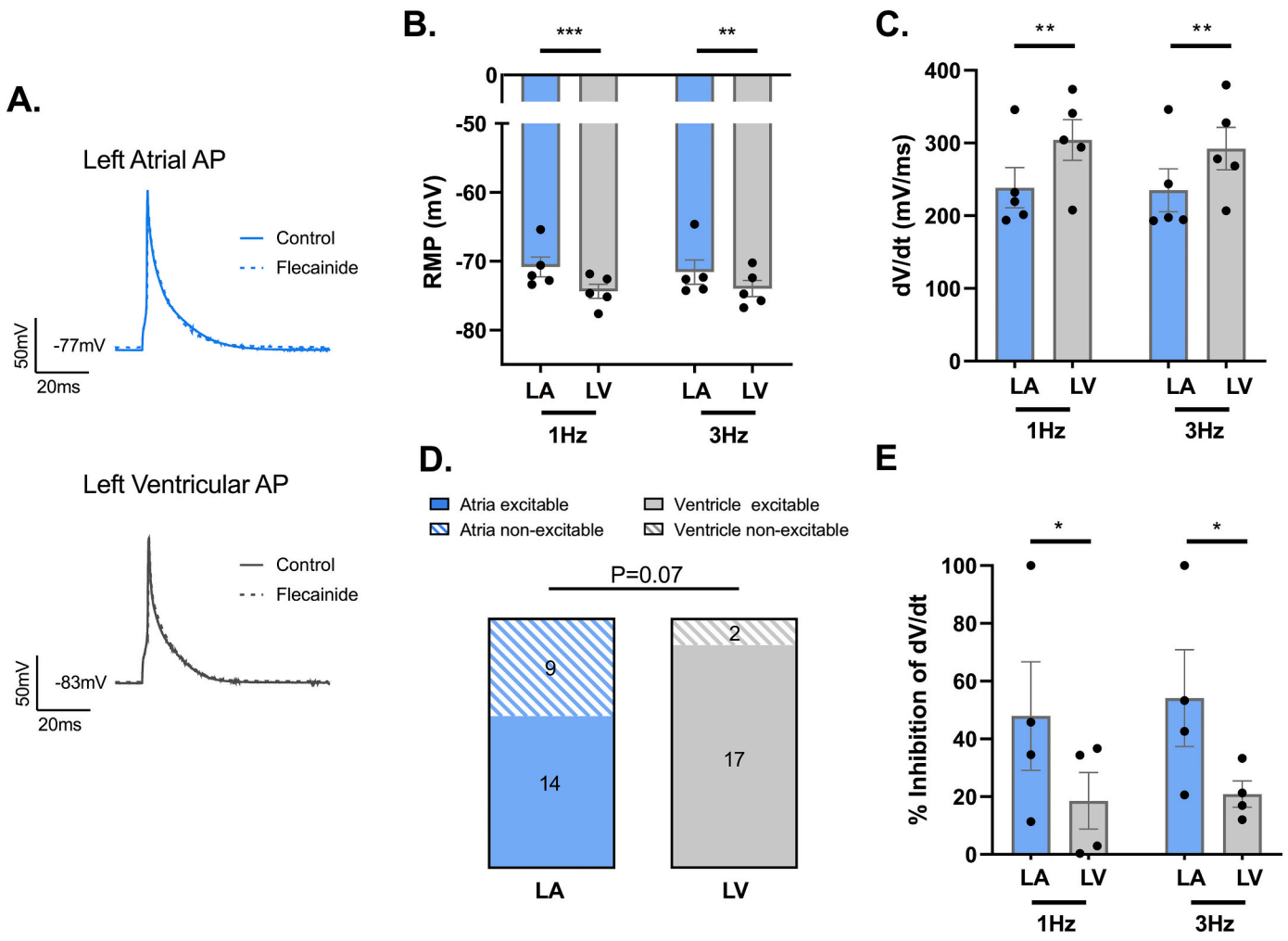

Fig. 4. Maximal upstroke velocity is higher in left ventricle (LV – grey bars) compared to left atrium (LA – blue bars) in single cardiac myocytes whilst LA myocytes are more sensitive to flecainide block (1 μM). A) Raw traces. B) Resting membrane potential of LA cells are significantly less negative than those of the LV at a variety of pacing cycle lengths (at 1 Hz, LA −70.8 ± 1.4 mV;LV -74.4 ± 1.0 mV $p = 0.0002$, $n = 23$–40/5 cells/mice.) Each dot represents average per mouse from at least 3 cells, **p < 0.01, ***$p < 0.001$, (Two-way ANOVA). C) Maximal upstroke velocity is higher in single ventricular cells when compared to atrial cells (at 1 Hz, LA 238.6 ± 27.7 mV/ms;LV 304.2 ± 27.9 mV/ms *$p = 0.0018$, n = 23–40/5 cells/mice) Each dot represents average per mouse from at least 3 cells, **p < 0.01, ***p < 0.001, (Two-way nested ANOVA). D) After application of flecainide only 14/23 atrial cells remained excitable, whereas 17/19 ventricular cells were still able to generate an action potential ($p = 0.07$, Fisher's Exact Test, n = 4 mice). E) Flecainide significantly decreased dV/dT to a greater extent in atrial cells (at 1 Hz 47.9 ± 18.8%) when compared to ventricle cells (At 1 Hz, 18.6 ± 9.8%, $p = 0.04$, Each dot represents average per mouse from at least 3 cells, Two way nested ANOVA, n = 4 animals). (For interpretation of the references to colour in this figure legend, the reader is referred to the web version of this article.)

(control) to 18.5 ± 1.6 pA/pF (flecainide), p < 0.0001 $n = 14/4$ cells/mice)). The enhanced action of flecainide on atrial cardiomyocytes was maintained over the entire range of holding voltages but was exaggerated at more positive, physiological potentials as seen in Fig. 5D. At the most negative holding potential, of -120 mV, I_{Na} was inhibited by 47.4 ± 4.6% and 33.6 ± 2.6% in the atrial and ventricular cardiomyocytes respectively ($p = 0.0126$ n = 11/6,14/3 cells/mice), whilst at a holding potential of −70 mV currents were inhibited by 75.9 ± 6.8% in the atrial and 44.4 ± 4.5% in the ventricular cardomyocytes ($p < 0.001$, n = 11/6,14/3 cells/mice), Fig. 5E,F. This indicates a greater intrinsic sensitivity of left atrial I_{Na} to flecainide as well as an exaggerated voltage dependence. Interestingly, flecainide also significantly slowed sodium channel recovery in atrial, but not ventricular cardiomyocytes (**Supplemental Fig. 4**).

When we applied the flecainide biophysical inhibitory effects on I_{Na} in the cell model simulations, a reduction of dV/dt to 55.6 mV/ms in the atria when compared to 93.64 mV/ms in the ventricle was calculated, at 1 Hz pacing cycle length. Collectively, these data indicate that flecainide has a greater effect on atrial I_{Na}. We also applied flecainide to single cells under current clamp conditions in atrial and ventricular cells (Fig. 4). Interestingly, when superfusing flecainide under experimental conditions only 14/23 atrial cells remained excitable, whereas 17/19 ventricular cells were still able to generate an action potential ($p = 0.07$, Fisher's Exact Test, $n = 4$ mice), indicating the increased effectiveness of flecainide in the atria (Fig. 4D**)**. When we considered all cells (and a block of an AP as 100% inhibition), flecainide significantly decreased dV/dT to a greater extent in atrial cells (paced at 1 Hz 47.9 ± 18.8%) when compared to ventricular cells (paced at 1 Hz, 18.6 ± 9.8%, $p = 0.04$, Two way ANOVA, n = 4 animals)(Fig. 4E**)**, commensurate with the modelling data**.**

2.3. Atria display slower conduction velocity and are more sensitive to flecainide

In order to confirm the earlier cellular and modelling findings, we set out to investigate whether conduction of electrical signals is different across matched murine left ventricle and left atria, using optical mapping (Fig. 6**)**. Fig. 6E illustrates that LA conduction velocities are

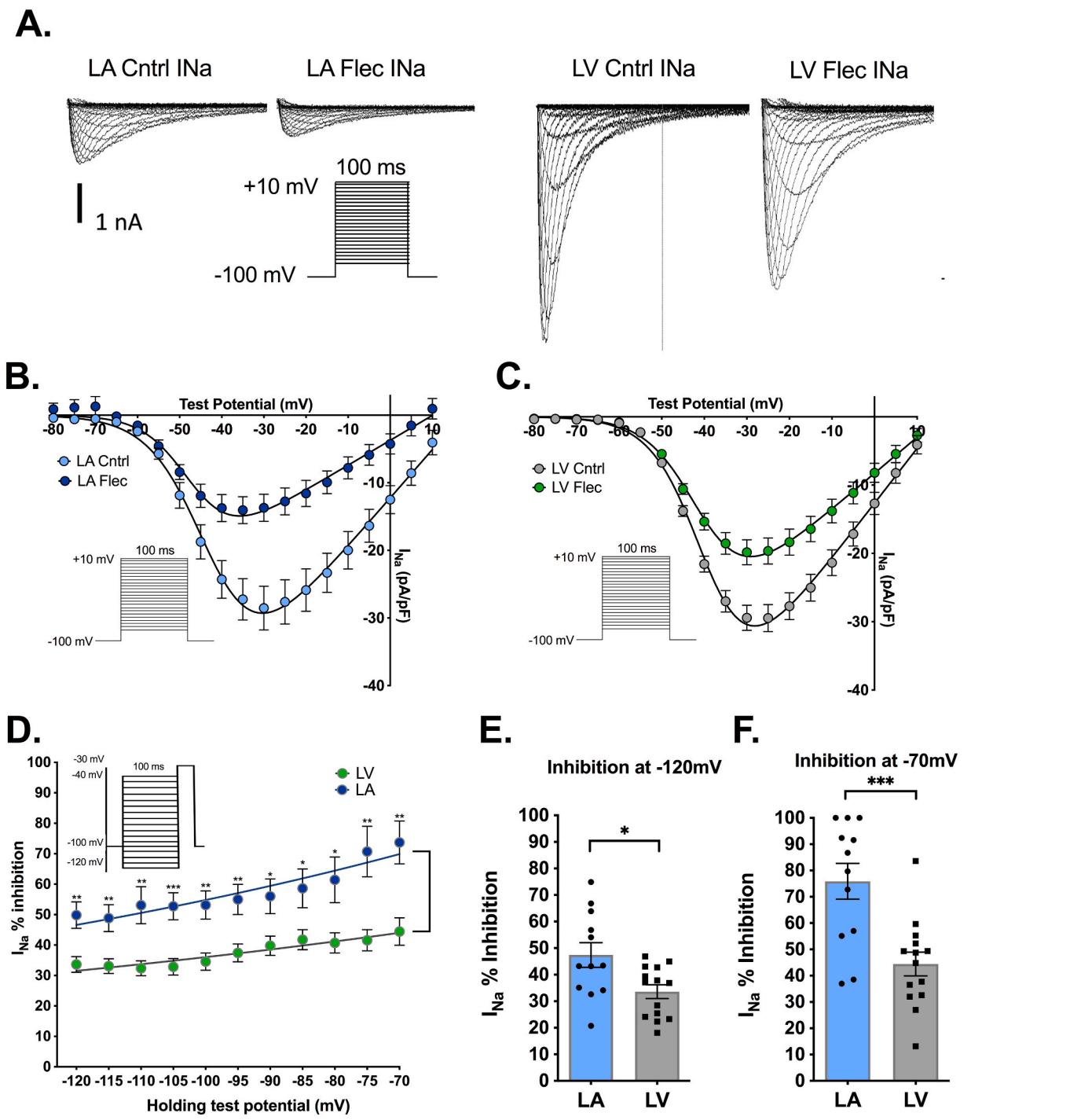

Fig. 5. Flecainide (1 μM) inhibits atrial I_{Na} to a greater extent than ventricular I_{Na}, which is more apparent at more positive holding potentials. A) Representative raw INa traces from left atrial (LA) and left ventricular (LV) cardiomyocytes with and without flecainide. Inset indicates voltage protocol. B) Current-voltage relationship of I_{Na} density in LA ($n = 11/6$ cells/mice) C) Current-voltage relationship of I_{Na} density in LV ($n = 14/4$ cells/mice). D) % inhibition of I_{Na} in left atrial (LA) and left ventricular (LV) cardiomyocytes from a variety of holding potentials, when stimulating I_{Na} by a voltage step to -30 mV. Inset indicates voltage protocol. E) LA and LV I_{Na} inhibition by flecainide from a holding potential of -120 mV. (LA = 75.9% ± 6.8; LV = 44.4% ± 4.5; ***p < 0.001) F) LA and LV I_{Na} inhibition from a holding potential of -70 mV (LA = 47.4% ± 4.6; LV = 33.6% ± 2.6). $n = 12/6$ cells/mice for LA and 14/4 for LV. Each dot represents an individual cell, **p < 0.01, ***p < 0.001, ****$p < 0.0001$ (Unpaired *t*-test).

significantly reduced compared to the LV at 10 Hz pacing cycle length (24.4 ± 2.7 vs 36.1 ± 6.2 cm/s, $p = 0.03$. $N = 5$). As expected, action potential duration was prolonged in the LV when compared to the LA (APD_{50} 27.1 ± 2.4 ms in the LV compared to 12.5 ± 0.8 ms in the LA, $p = 0.0011$, N = 5)(Figs. 6B, C).

In a separate set of experiments, we investigated if flecainide exerted differential effects on LA and LV CVs in the intact heart. In agreement with the cellular data, flecainide significantly decreased conduction in the left atrium (59.6 ± 7.2% of baseline) (Fig. 6F) whilst conduction was not significantly affected in the left ventricle (73.7 ± 4.7% of baseline) (Fig. 6G). Furthermore, no differences were seen in action potential duration between the two chambers after exposure to flecainide

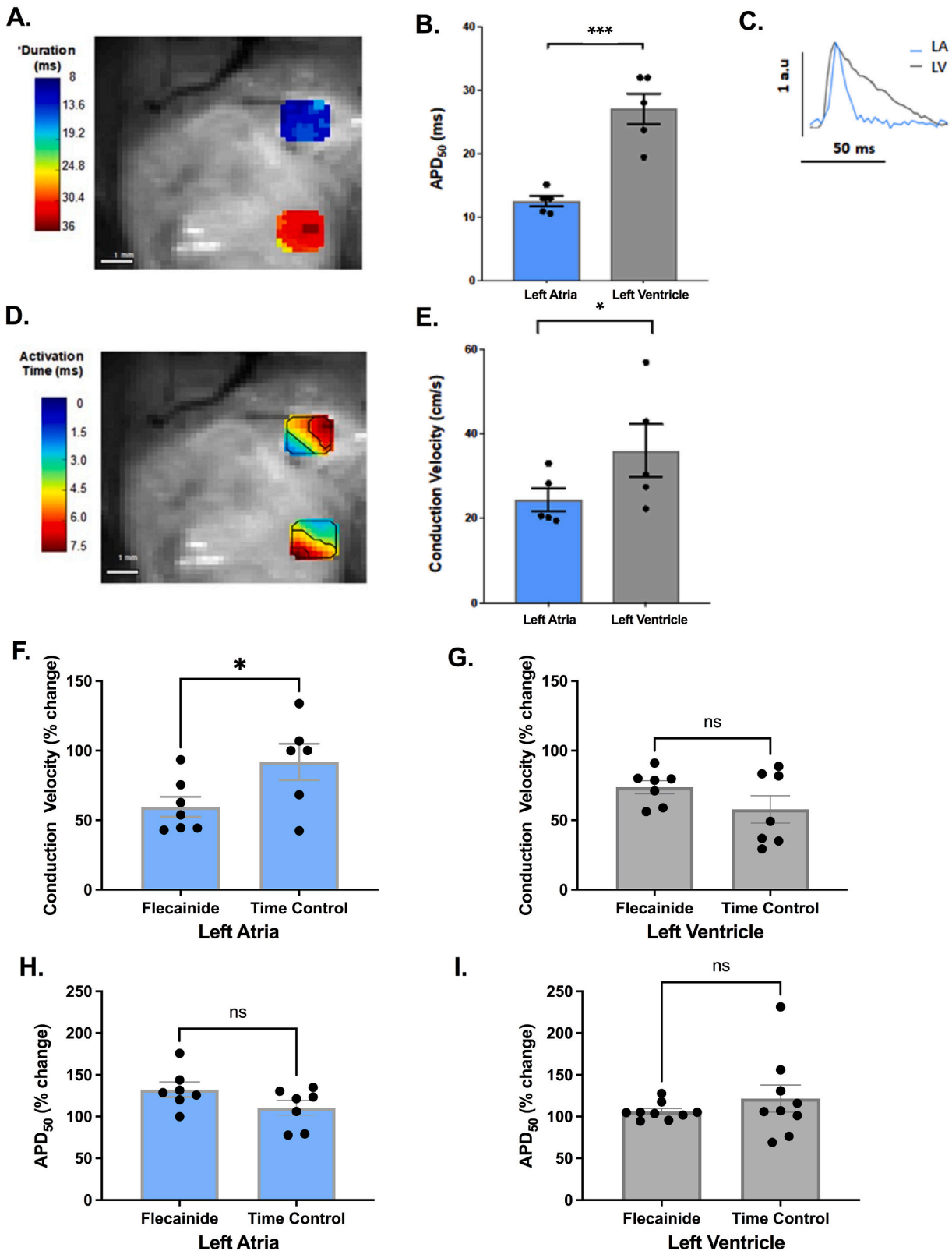

Fig. 6. Conduction velocities (CV) are reduced in left atria (LA) when compared to the left ventricles (LV), and are differentially affected by flecainide (1 μM) whilst APD is longer in LV. A) Representative action potential duration (APD50) maps recorded simultaneously from murine LA and LV tissue paced at 10 Hz. B) Grouped data of APD50 in LA (12.5 ± 0.8 ms) and LV (27.1 ± 2.4 ms, $p = 0.0011$, $N = 5$, two tailed student's *t*-test). Each dot represents an individual heart. C) Representative examples of APs recorded from the LA and LV. D) Representative CV maps in the LV compared to the LA. Contour lines are spaced by 2 ms. E) Grouped data of CV in LA (24.4 ± 2.7 cm/s) and LV (36.1 ± 6.2 cm/s, $p = 0.03$. N = 5, two tailed student's *t*-test). F) and G) Grouped data of CV in LA (F, light blue) and LV (G, grey) after the perfusion of flecainide and in comparison to time matched controls ($n = 7$–10). H) and I) Grouped data of APD in LA (H, light blue) and LV (I, grey) after the perfusion of flecainide and in comparison to time matched controls (n = 7–10). Each dot represents an individual heart. *p < 0.05, (two tailed student's t-test). (For interpretation of the references to colour in this figure legend, the reader is referred to the web version of this article.)

(Fig. 6H,I).

2.4. $Na_V1.5$, β2 and β4 subunits are differentially expressed in murine left atrium and left ventricle

We then determined whether potential differences in protein expression could explain the differing biophysical and pharmacological properties between the left atrium and the left ventricle. Specifically, we examined the expression of $Na_V1.5$, $Na_V\beta2$ and $Na_V\beta4$ in murine atrial and ventricular tissue, using Western blotting. $Na_V\beta2$ and $Na_V\beta4$ were previously demonstrated to affect activation, inactivation and recovery of I_{Na} [25]. As can be seen in Figs. 7A,D, $Na_V1.5$ showed a higher relative expression in the left atria when compared to the left ventricle in the mouse heart (LA = 3.18 ± 0.40 AU; LV = 1.00 ± 0.16 AU; $n = 13$, $p < 0.0001$). A number of additional bands of lower molecular weight were also noted on the Western blot, likely due to the polyclonal nature of the $Na_V1.5$ antibody (**Supplemental Fig. 5**). In contrast to this, both $Na_V\beta2$ (LA = 0.22 ± 0.03 AU; LV = 0.41 ± 0.05 AU; $n = 6$, $p = 0.0123$) and $Na_V\beta4$ (LA = 0.09 ± 0.003 AU; LV = 0.21 ± 0.01 AU; n = 6, p < 0.0001) were shown to be expressed at lower levels in the left atria when compared to the left ventricles (Figs. 7D,B,C).

2.5. SCN4B transcripts are decreased, whilst SCN5A are increased in left atrium compared to left ventricle in non-failing human heart tissue

Finally, we sought to determine if these findings in murine tissue are replicated in human tissue. To do so we conducted differential expression analysis on RNAseq from matched human left atrial and left ventricular tissue derived from 79 non-failing hearts. As seen in Fig. 7E,F, transcripts for *SCN5A,* the gene that encodes for $Na_V1.5$, was found at significantly higher levels in human left atria, compared to human left ventricles (1.66-fold change, $P_{adjusted} = 7.71*10^{-23}$), consistent with the murine expression data (Figs. 7A,D). Furthermore, transcript levels of *SCN4B,* which codes for $Na_V\beta4$, were significantly lower in human left atria when compared to the left ventricles (1.24-fold change, $p_{adjusted} = 0.0057$). *SCN2B* ($Na_V\beta2$) expression was modestly reduced in the left atria but this was not significant (1.09-fold change, $P_{adjusted} = 0.407$).

3. Discussion

The present findings demonstrate that flecainide exhibits some 'atrial-selective' inhibition of I_{Na} in the normal adult heart. These effects can explain the relatively low risk of ventricular pro-arrhythmia when flecainide is used in patients with atrial fibrillation. In more detail, the data demonstrate that: 1) left atrial tissue has slower conduction velocities then the left ventricle and is more sensitive to flecainide, when measured in the same heart; 2) Despite the left atrium expressing more *SCN5A*/$Na_V1.5$ protein then the left ventricle, at physiological membrane potentials, peak I_{Na} density is reduced in the atria; 3) The reduction in I_{Na} at physiological resting membrane potentials is sufficient to account for the decreased action potential upstroke velocity in the left atrium compared to the left ventricle; 4) Flecainide is more selective for left atrial I_{Na} compared to left ventricular cardiomyocytes; 5) Atrial peak I_{Na} density and sensitivity to flecainide is dramatically more influenced by resting membrane potential than the ventricular peak I_{Na} density. 6) Flecainide reduces the peak AP upstroke velocity more in atrial cells compared to ventricular cells.

3.1. Mechanisms promoting atrial susceptibility to arrhythmias

We robustly interrogated differential conduction velocities in the atria and ventricles by multi-vector, single-vector and activation time methodologies (**Supplemental Fig. 6)** [31]. Crucially, our optical mapping data compares atrial and ventricular recordings in the same heart. Conduction velocities recorded in our study are in the expected range, as demonstrated by others [32]. We demonstrate for the first time that mouse atrial tissue display circa 30% reduced conduction velocity compared to the ventricle, regardless of the methodology (multi vs single vector) utilized (Fig. 6**; Supplemental Fig. 6**). These data shed some light on the potential mechanisms contributing to enhanced atrial susceptibility for maintenance of re-entrant arrhythmias. In agreement with our data, van Veen et al. whilst employing electrogram array to record conduction in 3–4 months old mice, showed slightly lower conduction velocities in left atria (circa 30 cm/s) than the ventricles (circa 36 cm/s), though these were not directly compared [33]. Additionally, Thomas et al. detected a small but non-significant increase in conduction in mouse ventricles compared to the atria, using a liner epicardial electrode array [34].

Remarkably, reduced conduction in atria was observed despite a clear increase in $Na_V1.5$ protein expression in left atrial tissue, compared to left ventricle. Increased murine atrial $Na_V1.5$ expression was consistent with our data showing significantly increased expression of SCN5A in non-failing human left atrium, compared to left ventricle (Fig. 7). Consistent with these molecular biology findings, left atrial cardiomyocytes show increased peak I_{Na} compared to ventricular, when all sodium channels are activated, from a holding potential of −120 mV (Fig. 2A,C). Our patch clamp findings are in line with reports of others that use the holding potentials of −120 mV. Li et al. [24] were the first to describe marked increase in I_{Na} density in isolated atrial guinea pig cardiomyocytes when compared to ventricular epicardial cells. Similar findings have also been reported in rat, rabbit, and canine cardiomyocytes [23,25–27]. These studies have looked at the current density from a holding potential of −120 mV, when all channels are available, which is not the case under physiological conditions. Healthy ventricular cells have a resting membrane potential of between −65 and − 90 mV in situ whilst atrial cells are slightly more depolarized, sitting between −65 and − 80 mV [28,29]. In the present study we show that atrial peak I_{Na} density is differentially influenced by resting membrane potential, more so than observed in the ventricular cardiomyocyte (Fig. 2). Thus, at physiological resting membrane potentials, atria actually display a smaller peak I_{Na} density when compared to the ventricles. Consistent with the observed reduced peak I_{Na} in the left atrium, the action potential amplitude and V_{max} of atrial APs have been experimentally described as being between ≅ 150–300 V/s [35,36], compared with higher values of 250–450 V/s for human ventricular cells [37–39]. Similar differences appear to be conserved in smaller species [28,40,41]. Our modelling and cellular data consistently show a faster upstroke in the ventricle compared to the atria (Figs. 3 and 4), in agreement with the cardiac optical mapping studies (Fig. 6). With regards to the modelling data, we likely underestimate the impact of the reduced atrial I_{Na} on the upstroke, as we utilize a ventricular cell model and do not account for many other differences that exist between the atria and ventricle, such as the altered resting membrane potential. Since the magnitude of depolarizing I_{Na} is the key factor that determines conduction, a reduced I_{Na} at physiological membrane potentials is the most likely explanation for the slower conduction that we observed in the left atrium compared to the left ventricle (Fig. 6).

So, what determines the lower atrial I_{Na} at physiological membrane potentials, despite expression of a greater number of $Na_V1.5$ channels? Our patch clamp data demonstrate that left atrial cardiomyocytes display a greater negative shift in the voltage dependence of sodium channel inactivation (**Supplemental Fig. 2**). This is expected to result in a markedly reduced number of available $Na_v1.5$ channels, and a lower peak I_{Na}, when initiated from physiological holding potentials. We also detected a negative shift in atrial $V50_{act}$, meaning that the voltage at which half of the sodium channels are activated is more negative in the left atrial cardiomyocytes, when compared to the left ventricular cells (Fig. 1). This is in line with previous findings in rabbit cardiomyocytes [23]. It may be expected that a negative shift of the voltage dependence of sodium channel activation would decrease the voltage difference between the RMP and the activation threshold, leading to increased I_{Na} in the atria. However, this is counteracted by a greater negative shift in

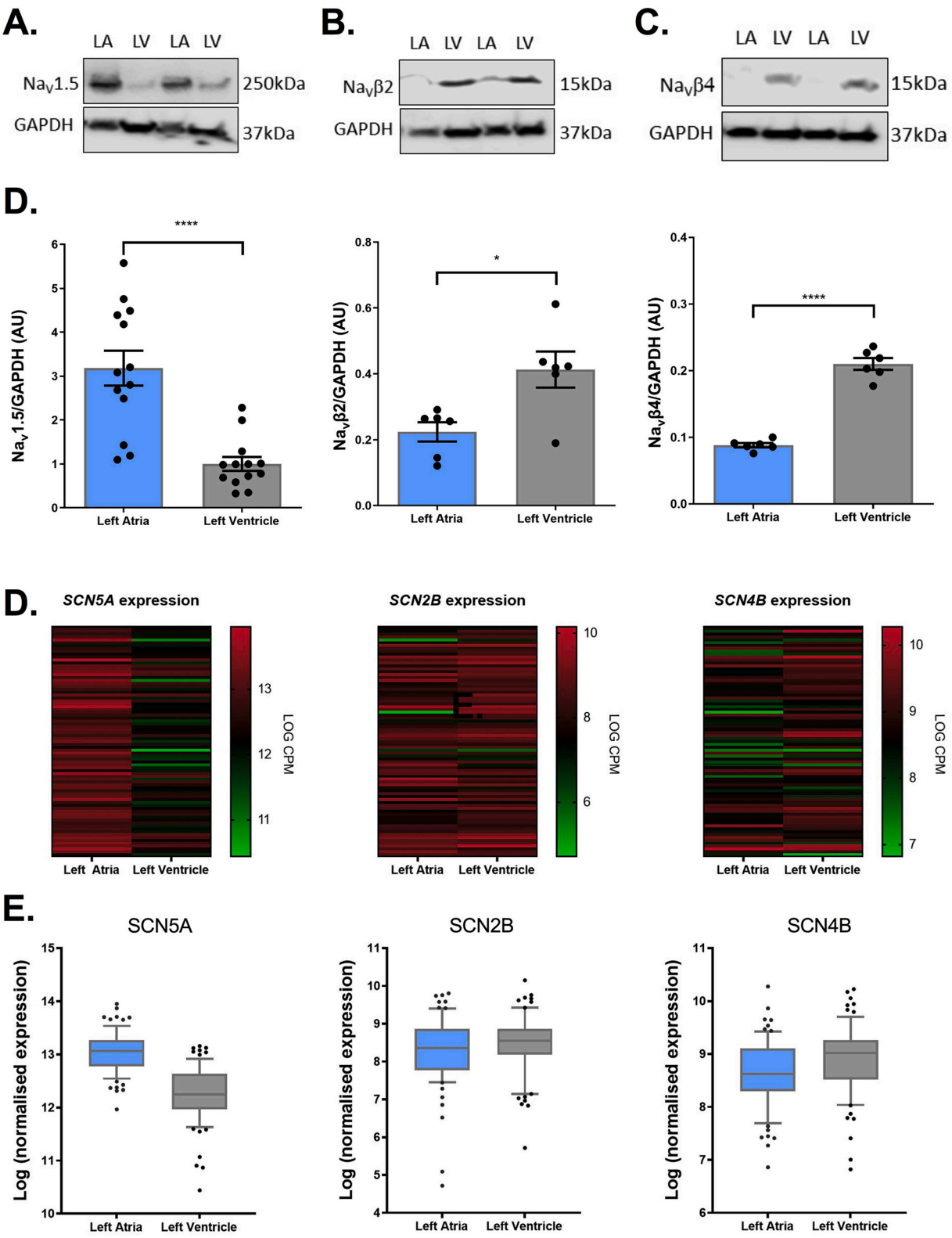

Fig. 7. Protein expression and RNAseq data of key sodium channel proteins in murine and human tissue. Western blots showing the protein expression of Na$_V$1.5 (A), Na$_V$β2 (B) and Na$_V$β4 (C) from murine left atrial (LA) and left ventricular (LV) samples. Na$_V$1.5 showed a higher relative expression in the LA, when compared to the LV (LA = 3.18 ± 0.40 AU; LV = 1.00 ± 0.16 AU; $n = 13$) ****$p < 0.0001$. Both Navβ2 (LA = 0.22 ± 0.03 AU; LV = 0.41 ± 0.05 AU; $n = 6$, *p < 0.05) and Na$_V$β4 (LA = 0.09 ± 0.003 AU; LV = 0.21 ± 0.01 AU; n = 6, *****p < 0.0001) are expressed at higher levels in the ventricle when compared to the atria. All blots were normalized to GAPDH. Each dot represents an individual heart, **p < 0.01, ***p < 0.001, ****p < 0.0001 (Two tailed Student's t-test). D) Heat maps illustrating the expression of *SCN5A*, *SCN2B*, and *SCN4B* from 79 paired patient samples from healthy LA and LV human tissue. E) Grouped data illustrating the RNAseq data for *SCN5A*, *SCN2B*, and *SCN4B*. *SCN5A* transcript levels were significantly higher in the LA when compared to the LV (adjusted $P = 7.71E\text{-}23$) whilst *SCN4B* transcript levels were significantly higher in the ventricle when compared to the atrium (adjusted $P = 0.0057$). No differences were seen in *SCN2B* transcript levels between the two chambers. Boxes represent the 25–75% and whiskers represent the min-max range, excluding outliers, which are shown as individual dots.

the voltage dependence of atrial sodium channel inactivation (**Supplemental Fig. 2**), resulting in a markedly reduced number of available $Na_v1.5$ channels, and a lower peak I_{Na} when initiated from physiological holding potentials. However, these data do not measure $V50_{act}$ at physiological membrane potentials thus it is difficult to predict the effects on peak I_{Na}.

The negative shift in $V50_{act}$ of the atrial sodium channels suggests an enhancement of excitability of atrial cardiomyocytes compared to ventricular cardiomyocytes. Negative shifts in the voltage dependence of I_{Na} activation permits channel activation with smaller depolarizations. This can result in premature activation of the sodium channels with minor depolarization. Although it has been shown here that there are a smaller proportion of left atrial sodium channels available for activation at physiologically relevant holding potentials, those that are available are potentially more sensitive to an untimely depolarization of membrane potential and may be more susceptible to premature activation.

Thus, the combined functional effects of the different biophysical properties of left atrial and left ventricular cardiomyocyte I_{Na} are a slowing of conduction velocity but an increased risk of ectopy. These effects are probably further magnified due to the more positive resting membrane potential in the atria compared to the ventricles, as illustrated in Fig. 4**B**. This may well account for the increased incidence of ectopy and re-entrant arrhythmia in the atria compared to ventricle although more work is required to validate this.

3.2. Do $Na_V\beta$-subunit expression differences mediate I_{Na} differences between the atria and ventricles?

Here we show that atrial expression of $Na_V\beta2$ and $Na_V\beta4$ is dramatically reduced in mouse hearts. In addition, RNAseq data from non-failing human hearts showed a similar pattern, reduction in transcript levels of *SCN2B* and *SCN4B* in the left atrium (Fig. 7). Chen et al., showed that kinetic properties of sodium channels co-expressing $Na_V1.5$ with $Na_V\beta2$ and $Na_V\beta4$ subunits were similar to those of the ventricular sodium channels, with more positive activation potential, more positive inactivation and faster recovery of the sodium channels. Equally, kinetic properties of sodium channels expressing $Na_V1.5$ alone were similar to those of the atrial sodium channels [25]. However, as experiments were performed in HEK293 cells co-expressing $Na_V\beta2$ and $Na_V\beta4$ subunits together, it is unclear whether the effects on channel kinetics required expression of both $Na_V\beta2$ and $Na_V\beta4$ or just one of the subunits. Indeed, Malhotra et al. showed that β2 had no detectable effects on channel kinetics using a heterologous expression system, suggesting that the effects of β2 may involve cell adhesion and cytoskeletal communication as opposed to channel gating [42]. Meanwhile, co-expression of the β4 subunit with $Na_V1.5$ resulted in a negative shift in the voltage dependence of inactivation when compared to $Na_V1.5$ alone [43]. Furthermore, mutations in both of these subunits have been associated with arrhythmogenic consequences [43,44]. In addition to β2 and β4 subunits Nav1.5 may also interact with β1 and β3 subunits, which have also been shown to modulate sodium channel activity [45,46]. Interestingly, recent work has illustrated that the loss of Scn1b ($Na_V\beta1$) in murine myocytes differentially affected the potencies of lidocaine and ranolazine, whilst also showing a distinct difference in transcriptional expression between human atria and ventricles [47] In the present study we did not investigate the effects of $Na_V\beta1$ and $Na_V\beta3$ expression on sodium channel function and localization, however, this should be an area of further study.

In addition to direct effects of β subunits on biophysical properties of I_{Na}, β subunits can also affect sodium channel localization. For AP conduction, location of $Na_V1.5$ on the cell membrane is particularly important, as are the number of channels in a particular cluster of channels as recently shown by Hichri et al. [48] Furthermore, work has shown that there are a number of different sub-pools of channels at the lateral membrane [49]. Whether β-subunits are involved in localization of channels to a particular microdomain remains to be investigated.

3.3. Flecainide effectiveness and the atria

Flecainide preferentially binds to sodium channels in the open state [50]. Our data adds to this knowledge by clearly showing that flecainide more effectively inhibits atrial I_{Na} across a range of holding potentials including physiological potentials. Several differences between atrial and ventricular tissue can explain this difference, including i) greater inhibition due to the difference in resting membrane potential [28], ii) greater inhibition of left atrial I_{Na} regardless of holding potential, and iii) greater inhibition of left atrial INa due to increased atrial expression of $Na_V\beta2$ and $Na_V\beta4$ subunits. Additionally, in vivo, greater inhibition is expected due to increased use dependence in fast-firing fibrillating atria.

It is well-known that the atrial resting membrane potential is more positive – depolarized – than the ventricular resting membrane potential [29,40] and this has also been shown in the current data set. Our data now add novel insights into the differences between atrial and ventricular sodium channel properties and expression profiles and suggest that these physiological differences lead to further inherent atrial selectivity of flecainide (Figs. 4, 5 and 6). We have previously shown that the extent of flecainide's I_{Na} inhibition is highly sensitive to small changes in atrial resting membrane potential, whilst our more recent work has shown that atrial RMP modifies the effectiveness of several clinically used AADs [28,51]. This sensitivity clearly contributes to the observed lower atrial I_{Na} at physiological membrane potentials. In addition, other factors affecting the differential effects of flecainide on $Na_V1.5$ channels in the atria and ventricles clearly exist. Whether the alterations in β-subunit chamber specific expression seen in this study contribute to differences in flecainide effectiveness remains unanswered. Further studies determining the supra-molecular clustering of sodium channels including their subunit on cardiomyocyte membranes are warranted. In murine *Scn3b*$^{-/-}$ hearts, where the β3 subunit is not expressed, flecainide produced reduced arrhythmic incidences combined with prolonged refractory periods and shortened APDs, despite the fact that these cardiomyocytes showed a reduction in I_{Na} and a negative shift in $Na_V1.5$ channel inactivation [52].

In light of our findings, atrial selectivity of flecainide in healthy myocardium is apparent and thus our data explain the lack of ventricular arrhythmias observed in Flec-SL and EAST-AFNET4 trials. The dosing regimens in these trials is not dissimilar to that of the CAST and CAST II trials so perhaps depolarization of the ventricular resting membrane potential during ischemia and in the border zone of myocardial infarctions enhanced flecainide effectiveness in "dangerous" areas in the left ventricle with scars (which were present in all patients in CAST and CAST II).

3.4. Limitations

While we verified key molecular changes in human tissue, this study was mainly performed in healthy mouse hearts. Validation in large mammals and human cardiomyocytes is warranted. We must also consider that our findings are relevant for hearts without structural heart disease, the main group of patients in whom sodium channel blockers are currently used, this study did not directly investigate the proarrhythmic effects of flecainide which are mainly found in infarcted hearts with structural heart disease or during ischemia. In addition to direct effects of β subunits on biophysical properties of I_{Na}, β subunits can also affect sodium channel clustering, a novel modulator of Nav1.5 function [48] It is conceivable that altered clustering contribute to the physiological differences between atrial and ventricular I_{Na} found here. In addition it has been shown that other alpha-subunits, such as Nav1.8, may contribute to cardiac conduction and mRNA for such proteins have been detected in both atrial and ventricular tissue [53]. How these may contribute to the chamber differences observed in this study is unclear. Furthermore, work has shown that there are a number of different sub-pools of channels at the lateral membrane [49]. Whether β-subunits are involved in localization of channels to a particular microdomain remains

to be investigated. Finally we also need to consider that it is not only the number of available channels at physiological diastolic potentials that will determine the conduction velocity but it can also be determined by other factors such as the density of gap junctions, sodium and calcium concentrations as well as cell geometry [54–56]. These factors go beyond the scope of the present study but should definitely be investigated in the future.

3.5. Conclusion and clinical significance

Our data illustrate the striking differences in the electrical properties of left atrial and ventricular myocardium. Of most clinical interest is demonstration that flecainide is more effective at inhibiting atrial sodium channels. Our findings can explain the good safety profile of sodium channel blockers in patients without myocardial scars, e.g. those with atrial fibrillation and with preserved left ventricular function, while also providing a reasonable explanation for the pro-arrhythmia seen in earlier studies in survivors of a myocardial infarction with heart failure with reduced ejection fraction. Determining the molecular drivers of the atrial and ventricular resting membrane potential and identifying the molecular interaction partners of flecainide and similar substances, may help to identify new targets for safe antiarrhythmic drug therapy. This is much needed to implement systematic, early rhythm control therapy in patients with AF.

4. Methods

4.1. Animal model

All experiments were conducted under the Animals (Scientific Procedures) Act 1986 and approved by the home office (PPL numbers 30/2967 and PFDAAF77F) and the institutional review board at the University of Birmingham.

4.2. Optical mapping of murine atria and ventricles

Mouse (CD-1, 29–49 g, Charles River, United Kingdom) hearts were isolated under deep isoflurane-induced inhalation anaesthesia (4% in O_2, 1.5 L min^{-1}). Optical mapping of mouse whole hearts was performed as previously described [57]. Mice were anesthetized using isoflurane (4% in 100% O2, 1.5 L min^{-1}). Hearts were removed and the aorta immediately cannulated. Hearts were Langendorff-perfused with an oxygenated (95% O2 5% CO2) crystalloid buffer solution containing (in mM) NaCl 114, KCl 4, CaCl2 1.4, NaHCO3 24, NaH2PO4 1.1, glucose 11 and sodium pyruvate 1 (pH 7.4, 37 °C) at a perfusion pressure of ca.80 mmHg. Potentiometric dye Di-4-ANEPPS (5 mg/mL. 25-100 μL) was loaded via bolus injection into the perfusion line over 3–5 min. Blebbistatin (12 μM) was added to the perfusate to prevent movement of the tissue during recording, whilst flecainide was added in the relevant experiments at 1 μM.

Hearts were paced at 10 Hz with 1 ms pulses from the right atrium epicardial surface using silver bipolar electrodes. Pulse amplitude was 2× the diastolic threshold. Hearts were illuminated during recordings by two dual LEDs (530 ± 25 nm) and emitted light collected at >630 nm. 10s recordings were acquired at 0.5 kHz at 51*51 pixel resolution using a Evolve Delta EMCCD camera (Photometrics, USA).

To ensure effective recording of the signals, sequential recordings were collected. Following recording of the anterior ventricular surface, the hearts were re-orientated. The atria were moved so they were in the focal plane and removed from the ventricles to prevent signal overlap. To enable direct comparison between the left atria and ventricle, a 9 × 9 pixel (1.4 cm2) region was analysed from both chambers (Fig. 1). Optical action potentials (APs) and conduction velocities (CV) were analysed using ElectroMap, as previously described [31].

4.3. Murine cardiomyocyte isolation

LA and LV murine cardiomyocytes were isolated from male and female adult mice (12–20 weeks old), bred on the 129/sv background, as previously described [28] . Briefly, hearts were removed under isoflurane-induced anaesthesia (4% in O_2, 1.5-3 L min^{-1}) and perfused at 4 ml/min at 37 °C on a vertical Langendorff apparatus with the following solutions, equilibrated with 100% O_2: (i) HEPES-buffered modified Tyrode's solution containing in mM: NaCl 145, KCl 5.4, $CaCl_2$ 1.8, $MgSO_4$ 0.83, Na_2HPO_4 0.33, HEPES 5 and glucose 11 (pH 7.4, NaOH); (ii) Ca^{2+}-free Tyrode's solution for 5 min; (iii) Tyrode's enzyme solution containing 20 μg/mL Liberase™ (Roche, Indianapolis, IN, for I_{Na} experiments) or 640 μg/ml collagenase type II, 600 μg/ml collagenase type IV and 50 μg/ml protease (Worthington, Lakewood, NJ, for AP recordings), 0.1% bovine serum albumin (BSA, Sigma), 20 mM taurine and 3-30 μM $CaCl_2$. The switch to a different enzyme solution for AP recordings was due to commercial availability. The heart was removed from the Langendorff and perfused with 5 ml of modified Kraft-Bruhe (KB) solution containing in mM: DL-potassium aspartate 10, L-potassium glutamate 100, KCl 25, KH_2PO_4 10, $MgSO_4$ 2, taurine 20, creatine 5, EGTA 0.5, HEPES 5, 0.1% BSA and glucose 20 (pH 7.2, KOH). Perfusion timings were between 10 and 25 min dependent on whether ventricular or atrial cells were being isolated and between hearts. The LA and LV chambers were dissected from the digested heart and placed into separate petri dishes containing 1 ml/2 ml respectively of the modified KB solution where they were manually disassociated using glass pipettes with increasing resistances. After dissociation was completed, Ca^{2+} was reintroduced in a stepwise manner over a period of 90 min to a final concentration of 1.8 mM for recordings of I_{Na} and 1 mM for AP recordings.

4.4. Electrophysiology

Dissociated mouse LA and LV cardiomyocytes were transferred to an initially static bath recording chamber and allowed to adhere to laminin-coated coverslips (10 mm diameter). Whole cell patch clamp recordings were obtained in voltage clamp mode using borosilicate glass pipettes (tip resistances 2.2–3 MΩ). All recordings and analysis protocols were performed using an Axopatch 1D amplifier (Molecular Devices, USA) and a CED micro1401 driven by Signal v6 software (CED, UK). Pipette solutions contained (mM): CsCl 115, NaCl 5, HEPES 10, EGTA 10, MgATP 5, $MgCl_2$ 0.5 and TEA 20 (pH 7.2, CsOH). To ensure adequate voltage control of I_{Na}, currents were recorded in a low sodium external solution containing in mM: NaCl 10, $C_5H_{14}ClNO$ 130, KCl 4.5, HEPES 10, $CaCl_2$ 1.8, $MgCl_2$ 1.2 and glucose 10 (pH 7.4, CsOH).L-type Ca^{2+} current was blocked with 2 mM $NiCl_2$. Experiments were performed at 22 ± 0.5 °C. I_{Na} was recorded before and after the addition of flecainide (1 μM). Current signals were sampled at 50 kHz and low pass filtered at 20 kHz. I_{Na} was normalized to cell capacitance and expressed as pA/pF. To assess current-voltage relationships, I_{Na} was elicited using 100 ms step depolarizations at 1 Hz over a test potential range of -95 mV to +10 mV, in 5 mV increments, from a holding potential of -100 mV. I/V curves were fitted using the modified Boltzmann equation as described previously [58] . Measurements of steady state inactivation of I_{Na}, were made by applying pre-pulses ranging from −120 to −40 mV in 5 mV increments for 500 ms prior to the test potential (−30 mV for 100 ms). As well as being able to calculate V_{50} inactivation voltages, this protocol also allowed for measurements of I_{Na} at different holding voltages. This also allowed for measurements of instantaneous I_{Na} inhibition by flecainide across a range of different holding voltages which could then be compared between atrial and ventricular cardiomyocytes. For recording of action potentials whole cell patch clamp recordings were obtained in current clamp mode. Pipette solutions contained (mM): 130 K^+ glutamate, 10 NaCl, 10 KCl, 0.5 $MgCl_2$, 5 MgATP, 10 HEPES (pH 7.2, CsOH). The external solution contained (mM): 145 NaCl, 5.4 KCl, 0.83 $MgSO_4.7H_20$, 0.33 NaH_2PO_4, 5 HEPES, 11 Glucose, 1 $CaCl_2$, 1.2 $MgCl_2$

(pH 7.4, CsOH). Experiments were performed at 37 ± 0.5 °C. Action potentials were stimulated via the pipette using a stimulus of at least twice diastolic threshold, at frequencies of 1 and 3 Hz, for a duration of 1 ms. Following baseline recordings, cells were superfused with 1 μM flecainide for 5 min before repeating the recordings. Action potential characteristics were measured using modified algorithms from the ElectroMap software as previously described [51]. Following 60 s pacing to reach steady state, resting membrane potential (RMP) was defined as the minimum diastolic membrane potential. Maximum upstroke velocity (dV/dt) was measured as the maximum derivative of the action potential recording.

4.5. Biophysical modelling

Full details for the modelling methodology and data can be found in the supplement. In brief, sodium channel activation and inactivation protocols were fitted to a standard Hodgkin and Huxley formulation of the I_{Na} channel:

$$I_{Na} = G_{Na} m^3 hj(V - E_{Na})$$

G_{Na} is the maximum channel conductance, m is the activation gating variable, h and j are inactivation gating variables, V is the membrane potential, E_{Na} is the sodium Nernst potential. We assume j and h are equivalent as insufficient data is available to fit distinct inactivation gates. The gating variables were fitted to activation and inactivation data for atria and ventricles.

Flecainide inhibition is dependent on the holding potential and is distinct for the atria and ventricle. To approximate flecainide effects, we introduced a linear scalar that represented sodium channel inhibition. We fitted this scalar to inhibition data for atria and ventricle sodium channels. To predict the impact of different sodium ion channel kinetics on emergent action potential morphology, we introduced the fitted atrial and ventricle sodium channel models into the mouse variant of the Pandit ventricular myocyte model [30]. We used the same model for both the atria and ventricle sodium channel model.

4.6. Western blotting

Tissue samples were homogenised in homogenisation buffer (Tris adjusted to pH 7.3, 1 protease cocktail inhibitor tablet (Roche Diagnostics; complete ULTRA Tablets, Mini, EASYpack) diluted in 10 mL buffer, with phosphatase cocktail inhibitor 2 and 3 (Sigma) added (both 1:100 concentration). The homogenisation buffer was added to the tubes containing the.

tissue in a ratio of 1 mg of tissue: 10uL of buffer and homogenised using the Precellys® system (Bertin Instruments). Samples were then centrifuged and 10uL of sample (≈15μg of protein) was loaded onto 4–15% gradient Mini-PROTEAN® TGXTM gels (Bio-Rad) immersed in running buffer (0.025 M Tris base, 0.19 M glycine and 0.1% *w/v* sodium dodecyl sulphate). Proteins were transferred onto polyvinylidene difluoride membranes (Bio-Rad). The membrane was then blocked with 5% milk powder dissolved in PBS-T overnight at 4 °C. Blocked membranes were then incubated for an hour with antibodies for $Na_V1.5$ (1:200, Alomone, ASC-005), $Na_V\beta2$ (1:400, Alomone, ASC-007), $Na_V\beta4$ (1:800, Alomone, ASC-044) and GAPDH (1:4000, ThermoFisher Scientific, AM4300). After washing, membranes were then incubated for 1 h at room temperature with the appropriate horseradish peroxidase linked conjugated secondary IgG antibodies (1:7500, GE Healthcare NA934V or 1:4000, GE Healthcare NA931V) diluted in 5% milk powder in PBS-T at room temperature.

For detection membranes were submerged in 5 ml of detection reagent (GE Healthcare, ECL Western Blotting Detection Reagents, Amersham) whilst the Odyssey Fc Imaging System (LICOR) was utilized to measure densitometry to monitor the level of protein expression. Raw densitometry values were normalized to GAPDH.

4.7. RNAseq

Kallisto (version 0.42.3) was used to quantify the transcripts in all experiments [59]. To generate an indexed transcriptome for performing pseudoalignments, we downloaded the human cDNA file Homo_sapiens.GRCh38.cdna.all.fa.gz from Ensembl (ftp://ftp.ensembl.org/pub/release-91/fasta/homo_sapiens/cdna/). This compressed FASTA file was made into an indexed transcriptome using the command "kallisto index" and this file was subsequently used for all transcript quantification. RNA-seq data derived from 79 pairs of adult matched LA and LV tissue was utilized (dbGaP accession phs001539.v1.p1 for left atrium, GEO accession GSE141910 for LV, **Online Table 1**) to assess differences and similarities between the chambers.

After quantification of transcript abundance using kallisto, we used the tximport package to import quantification data into the DEseq2 package in R [60,61]. To collapse transcripts into gene level summaries, we used the "hsapiens_gene_ensembl" repository through the R package biomaRt [62]. Only genes with at least 10 counts across the row were retained to filter noise at the low end of the distribution of transcript abundance. To identify DE genes, we used the function "DESeqDataSetFromTximport" to ingest the filtered data, then the function "results" to produce lists of DE genes. Unadjusted *P*-values are produced using the Wald test, and P-values are adjusted for multiple testing corrections using Benjamini-Hochberg. We used the DEseq2 function lfcShrink to transform expression values to log2 scale. All analyses were performed in R using version 3.5.1.

4.8. Statistical analyses

Data are expressed as mean ± standard error, unless otherwise stated. Data were checked for normal distribution and statistical analysis was performed using (un)paired Student *t*-tests or two-way (nested) ANOVA with Tukey post-hoc as appropriate. Countables, such as number of excitable vs non-excitable cells, were tested using the Fisher's exact test. Significance was taken as two-sided $P < 0.05$, and all analysis was carried out in GraphPad Prism 9.0.

Author contributions

S.O·B and A.P·H are first co-authors as they have provided equal contributions to this work. S.O·B, A.P·H and D.P. designed the study. S.O·B and A.P·H carried out and analysed the electrophysiological studies and together with C.A and J.S.R carried out the molecular biology experiments. C.O·S. and S·N·K carried out and analysed the optical mapping recordings, and C.O.S also developed algorithms data analysis. M.O.R carried out and analysed the current clamp recordings. A.A and S.N built the myocyte model and carried out the computer modelling. N.T, A.P.H and P.T.E carried out the RNAseq experiments and analysis. D.P, D.M.J. S.O·B, M.O.R, S.N·K and A.A prepared figures. D.M.J. and D.P wrote the manuscript.

Declaration of Competing Interest

P.T.E. receives sponsored research support from Bayer AG and IBM Health, and has consulted for Novartis, Quest Diagnostics, Bayer AG and MyoKardia.

Acknowledgements

This work was funded by the British Heart Foundation (PG/17/55/33087 to D.P. and P.K.; RG/17/15/33106 to D.P.; FS/19/12/34204 to D.P.; FS/19/16/34169 to D.P.; PG/17/30/32961 to P.K. and A.P·H.; Accelerator Award AA/18/2/34218 to P.K. and L.F.; FS/13/43/30324 to P.K. and L.F.), European Union (grant agreement No 633196 [CATCH ME] to P.K. and L.F.), grant agreement No 965286 [MAESTRIA] to L.F., and Leducq Foundation to P.K. This work was also supported by a grant

from the American Heart Association to P.T.E (18SFRN34110082) and an AHA SFRN postdoctoral fellowship to A.W.H. PK receives further support from the DZHK.

Appendix A. Supplementary data

Supplementary data to this article can be found online at https://doi.org/10.1016/j.yjmcc.2022.01.009.

References

[1] B.P. Krijthe, et al., Projections on the number of individuals with atrial fibrillation in the European Union, from 2000 to 2060, Eur. Heart J. 34 (2013) 2746–2751.
[2] Y. Miyasaka, et al., Secular trends in incidence of atrial fibrillation in Olmsted County, Minnesota, 1980 to 2000, and implications on the projections for future prevalence, Circulation 114 (2006) 119–125.
[3] D.S. Echt, et al., Mortality and morbidity in patients receiving encainide, flecainide, or placebo, N. Engl. J. Med. 324 (1991) 781–788.
[4] P. Kirchhof, et al., Short-term versus long-term antiarrhythmic drug treatment after cardioversion of atrial fibrillation (Flec-SL): a prospective, randomised, open-label, blinded endpoint assessment trial, Lancet 380 (2012) 238–246.
[5] P. Kirchhof, et al., Improving outcomes in patients with atrial fibrillation: rationale and design of the early treatment of atrial fibrillation for stroke prevention trial, Am. Heart J. 166 (2013) 442–448.
[6] C.T. January, et al., 2019 AHA/ACC/HRS focused update of the 2014 AHA/ACC/HRS guideline for the management of patients with atrial fibrillation: a report of the American College of Cardiology/American Heart Association Task Force on Clinical Practice Guidelines and the Heart Rhythm Society, J. Am. Coll. Cardiol. 74 (2019) 104–132.
[7] D.L. Packer, et al., Effect of catheter ablation vs antiarrhythmic drug therapy on mortality, stroke, bleeding, and cardiac arrest among patients with atrial fibrillation: the CABANA randomized clinical trial, JAMA 321 (2019) 1261–1274.
[8] P. Kirchhof, et al., 2016 ESC guidelines for the management of atrial fibrillation developed in collaboration with EACTS, Eur. Heart J. 37 (2016) 2893–2962.
[9] P. Kirchhof, et al., Early rhythm-control therapy in patients with atrial fibrillation, N. Engl. J. Med. (2020), https://doi.org/10.1056/NEJMoa2019422.
[10] A. Rillig, et al., Early rhythm control therapy in patients with atrial fibrillation and heart failure, Circulation 144 (2021) 845–858.
[11] Lei Ming, Lin Wu, A. Terrar Derek, L.-H. Huang Christopher, Modernized classification of cardiac antiarrhythmic drugs, Circulation **138** (2018) 1879–1896.
[12] K.R. DeMarco, C.E. Clancy, Cardiac Na channels: structure to function, Curr. Top. Membr. 78 (2016) 287–311.
[13] J.R. Balser, The cardiac sodium channel: gating function and molecular pharmacology, J. Mol. Cell. Cardiol. 33 (2001) 599–613.
[14] A.A. Paul, H.J. Witchel, J.C. Hancox, Inhibition of the current of heterologously expressed HERG potassium channels by flecainide and comparison with quinidine, propafenone and lignocaine, Br. J. Pharmacol. 136 (2002) 717–729.
[15] C.H. Follmer, T.J. Colatsky, Block of delayed rectifier potassium current, IK, by flecainide and E-4031 in cat ventricular myocytes, Circulation 82 (1990) 289–293.
[16] W.J. Brackenbury, L.L. Isom, Na+ channel β subunits: overachievers of the ion channel family, Front. Pharmacol. 2 (2011).
[17] K.-H. Chen, et al., Distinctive property and pharmacology of voltage-gated sodium current in rat atrial vs ventricular myocytes, Heart Rhythm. 13 (2016) 762–770.
[18] S.C. Salvage, et al., Multiple targets for flecainide action: implications for cardiac arrhythmogenesis, Br. J. Pharmacol. 175 (2018) 1260–1278.
[19] D. Jiang, et al., Structure of the cardiac Sodium Channel, Cell 180 (2020) 122–134.e10.
[20] Paulus F. Kirchhof, Fabritz C. Larissa, Michael R. Franz, Postrepolarization refractoriness versus conduction slowing caused by class I antiarrhythmic drugs, Circulation 97 (1998) 2567–2574.
[21] J. Tamargo, A. Capucci, P. Mabo, Safety of flecainide, Drug Saf. 35 (2012) 273–289.
[22] K.T. Cragun, S.B. Johnson, D.L. Packer, Beta-adrenergic augmentation of flecainide-induced conduction slowing in canine Purkinje fibers, Circulation 96 (1997) 2701–2708.
[23] R.E. Caves, et al., Atrial-ventricular differences in rabbit cardiac voltage-gated Na + currents: basis for atrial-selective block by ranolazine, Heart Rhythm. 14 (2017) 1657–1664.
[24] G.-R. Li, C.-P. Lau, A. Shrier, Heterogeneity of sodium current in atrial vs epicardial ventricular myocytes of adult Guinea pig hearts, J. Mol. Cell. Cardiol. 34 (2002) 1185–1194.
[25] K.-H. Chen, et al., Distinctive property and pharmacology of voltage-gated sodium current in rat atrial vs ventricular myocytes, Heart Rhythm. 13 (2016) 762–770.
[26] Burashnikov Alexander, M. Di Diego José, C. Zygmunt Andrew, Belardinelli Luiz, Antzelevitch Charles, Atrium-selective sodium channel block as a strategy for suppression of atrial fibrillation, Circulation 116 (2007) 1449–1457.
[27] X. Fan, et al., Atrial-selective block of sodium channels by acehytisine in rabbit myocardium, J. Pharmacol. Sci. 132 (2016) 235–243.
[28] F. Syeda, et al., PITX2 modulates atrial membrane potential and the antiarrhythmic effects of sodium-channel blockers, J. Am. Coll. Cardiol. 68 (2016) 1881–1894.
[29] S.V. Pandit, Ionic mechanisms of atrial action potentials, in: Cardiac Electrophysiology: From Cell to Bedside, Elsevier, 2018, pp. 293–303, https://doi.org/10.1016/B978-0-323-44733-1.00031-6.
[30] S.V. Pandit, R.B. Clark, W.R. Giles, S.S. Demir, A mathematical model of action potential heterogeneity in adult rat left ventricular myocytes, Biophys. J. 81 (2001) 3029–3051.
[31] C. O'Shea, et al., ElectroMap: high-throughput open-source software for analysis and mapping of cardiac electrophysiology, Sci. Rep. 9 (2019) 1389.
[32] S. Kaese, S. Verheule, Cardiac electrophysiology in mice: a matter of size, Front. Physiol. 3 (2012).
[33] Toon A.B. van Veen, et al., Impaired impulse propagation in Scn5a-knockout mice, Circulation 112 (2005) 1927–1935.
[34] Suma A. Thomas, et al., Disparate effects of deficient expression of Connexin43 on atrial and ventricular conduction, Circulation 97 (1998) 686–691.
[35] S. Loose, et al., Effects of IKur blocker MK-0448 on human right atrial action potentials from patients in sinus rhythm and in permanent atrial fibrillation, Front. Pharmacol. 5 (2014).
[36] A.A. Dawodu, et al., The shape of human atrial action potential accounts for different frequency-related changes in vitro, Int. J. Cardiol. 54 (1996) 237–249.
[37] E. Drouin, F. Charpentier, C. Gauthier, K. Laurent, H.L. Marec, Electrophysiologic characteristics of cells spanning the left ventricular wall of human heart: evidence for presence of M cells, J. Am. Coll. Cardiol. 26 (1995) 185–192.
[38] Y. Péréon, et al., Differential expression of KvLQT1 isoforms across the human ventricular wall, Am. J. Phys. Heart Circ. Phys. 278 (2000) H1908–H1915.
[39] V. Iyer, R. Mazhari, R.L. Winslow, A computational model of the human left-ventricular epicardial myocyte, Biophys. J. 87 (2004) 1507–1525.
[40] D.A. Golod, R. Kumar, R.W. Joyner, Determinants of action potential initiation in isolated rabbit atrial and ventricular myocytes, Am. J. Phys. 274 (1998) H1902–H1913.
[41] C.A. Remme, et al., Overlap syndrome of cardiac sodium channel disease in mice carrying the equivalent mutation of human *SCN5A* -1795insD, Circulation 114 (2006) 2584–2594.
[42] Malhotra Jyoti Dhar, et al., Characterization of sodium channel α- and β-subunits in rat and mouse cardiac myocytes, Circulation **103** (2001) 1303–1310.
[43] A. Medeiros-Domingo, et al., SCN4B-encoded sodium channel beta4 subunit in congenital long-QT syndrome, Circulation 116 (2007) 134–142.
[44] H. Watanabe, et al., Mutations in sodium channel Beta1 and Beta2 subunits associated with atrial fibrillation, Circ. Arrhythm. Electrophysiol. 2 (2009) 268–275.
[45] N. Edokobi, L.L. Isom, Voltage-gated sodium channel β1/β1B subunits regulate cardiac physiology and pathophysiology, Front. Physiol. 9 (2018) 351.
[46] P. Angsutararux, W. Zhu, T.L. Voelker, J.R. Silva, Molecular pathology of Sodium Channel Beta-subunit variants, Front. Pharmacol. 12 (2021), 761275.
[47] W. Zhu, et al., Modulation of the effects of class Ib antiarrhythmics on cardiac NaV1.5-encoded channels by accessory NaVβ subunits. *JCI*, Insight 6 (2021), 143092.
[48] E. Hichri, H. Abriel, J.P. Kucera, Distribution of cardiac sodium channels in clusters potentiates ephaptic interactions in the intercalated disc, J. Physiol. 596 (2018) 563–589.
[49] J.-S. Rougier, et al., A distinct pool of Nav1.5 channels at the lateral membrane of murine ventricular cardiomyocytes, Front. Physiol. 10 (2019).
[50] E. Ramos, M.E. O'Leary, State-dependent trapping of flecainide in the cardiac sodium channel, J. Physiol. 560 (2004) 37–49.
[51] A.P. Holmes, et al., Atrial resting membrane potential confers sodium current sensitivity to propafenone, flecainide and dronedarone, Heart Rhythm. (2021), https://doi.org/10.1016/j.hrthm.2021.03.016.
[52] P. Hakim, R. Thresher, A.A. Grace, C.L.-H. Huang, Effects of flecainide and quinidine on action potential and ventricular arrhythmogenic properties in Scn3b knockout mice, Clin. Exp. Pharmacol. Physiol. 37 (2010) 782–789.
[53] T. Yang, et al., Blocking Scn10a channels in heart reduces late sodium current and is antiarrhythmic, Circ. Res. 111 (2012) 322–332.
[54] S.A. George, P.J. Calhoun, R.G. Gourdie, J.W. Smyth, S. Poelzing, TNFα modulates cardiac conduction by altering electrical coupling between myocytes, Front. Physiol. 8 (2017) 334.
[55] D.R. King, et al., The conduction velocity-potassium relationship in the heart is modulated by sodium and calcium, Pflugers Arch. 473 (2021) 557–571.
[56] R. Veeraraghavan, et al., Sodium channels in the Cx43 gap junction perinexus may constitute a cardiac ephapse: an experimental and modeling study, Pflugers Arch. 467 (2015) 2093–2105.
[57] C. O'Shea, et al., High-throughput analysis of optical mapping data using ElectroMap, JoVE (J. Visual Exp.) e59663 (2019), https://doi.org/10.3791/59663.
[58] M. Ackers-Johnson, et al., A simplified, Langendorff-free method for concomitant isolation of viable cardiac myocytes and nonmyocytes from the adult mouse heart, Circ. Res. 119 (2016) 909–920.
[59] N.L. Bray, H. Pimentel, P. Melsted, L. Pachter, Near-optimal probabilistic RNA-seq quantification, Nat. Biotechnol. 34 (2016) 525–527.
[60] C. Soneson, M.I. Love, M.D. Robinson, Differential analyses for RNA-seq: transcript-level estimates improve gene-level inferences, F1000Res 4 (2015) 1521.
[61] M.I. Love, W. Huber, S. Anders, Moderated estimation of fold change and dispersion for RNA-seq data with DESeq2, Genome Biol. 15 (2014) 550.
[62] S. Durinck, P.T. Spellman, E. Birney, W. Huber, Mapping identifiers for the integration of genomic datasets with the R/Bioconductor package biomaRt, Nat. Protoc. 4 (2009) 1184–1191.